ADVANCED MATERIALS
www.advmat.de

Observation of Yu–Shiba–Rusinov States in Superconducting Graphene

*Eva Cortés-del Río, Jose Luis Lado, Vladimir Cherkez, Pierre Mallet, Jean-Yves Veuillen, Juan Carlos Cuevas, José María Gómez-Rodríguez, Joaquín Fernández-Rossier, and Iván Brihuega**

When magnetic atoms are inserted inside a superconductor, the superconducting order is locally depleted as a result of the antagonistic nature of magnetism and superconductivity. Thereby, distinctive spectral features, known as Yu–Shiba–Rusinov states, appear inside the superconducting gap. The search for Yu–Shiba–Rusinov states in different materials is intense, as they can be used as building blocks to promote Majorana modes suitable for topological quantum computing. Here, the first observation of Yu–Shiba–Rusinov states in graphene, a non-superconducting 2D material, and without the participation of magnetic atoms, is reported. Superconductivity in graphene is induced by proximity effect brought by adsorbing nanometer-scale superconducting Pb islands. Using scanning tunneling microscopy and spectroscopy the superconducting proximity gap is measured in graphene, and Yu–Shiba–Rusinov states are visualized in graphene grain boundaries. The results reveal the very special nature of those Yu–Shiba–Rusinov states, which extends more than 20 nm away from the grain boundaries. These observations provide the long-sought experimental confirmation that graphene grain boundaries host local magnetic moments and constitute the first observation of Yu–Shiba–Rusinov states in a chemically pure system.

1. Introduction

Superconducting (SC) order arises in many materials because of the formation of a coherent many-body state of electrons pairs with zero spin.[1] The addition or removal of one electron from this state, resulting in an unpaired electron, costs a small energy gap associated to the overhead of breaking a pair. Interactions that promote magnetism tend to destroy superconducting order in most materials. When perturbed with magnetic impurities, the superconducting order is depleted locally, which can give rise to the appearance of the in-gap bound states known as Yu–Shiba–Rusinov (YSR) states.[2–4]

The measurement of YSR states on Mn adatoms on a superconductor, by means of scanning tunneling microscopy and spectroscopy (STM/STS), provided[5] the first direct observation of magnetism on an individual atom, as Anderson's theorem[6] precludes the existence of in-gap

E. Cortés-del Río, Prof. J. M. Gómez-Rodríguez, Prof. I. Brihuega
Departamento Física de la Materia Condensada
Universidad Autónoma de Madrid
Madrid E-28049, Spain
E-mail: ivan.brihuega@uam.es

Prof. J. L. Lado
Department of Applied Physics
Aalto University
Espoo 02150, Finland

Dr. V. Cherkez, Prof. P. Mallet, Prof. J.-Y. Veuillen
Université Grenoble Alpes
Grenoble 38000, France

Dr. V. Cherkez, Prof. P. Mallet, Prof. J.-Y. Veuillen
CNRS
Institut Neel
Grenoble F-38042, France

The ORCID identification number(s) for the author(s) of this article can be found under https://doi.org/10.1002/adma.202008113.

DOI: 10.1002/adma.202008113

Prof. J. C. Cuevas
Departamento Física Teórica de la Materia Condensada
Universidad Autónoma de Madrid
Madrid E-28049, Spain

Prof. J. C. Cuevas, Prof. J. M. Gómez-Rodríguez, Prof. I. Brihuega
Condensed Matter Physics Center (IFIMAC)
Universidad Autónoma de Madrid
Madrid E-28049, Spain

Prof. J. M. Gómez-Rodríguez, Prof. I. Brihuega
Instituto Nicolás Cabrera
Universidad Autónoma de Madrid
Madrid E-28049, Spain

Prof. J. Fernández-Rossier
QuantaLab
International Iberian Nanotechnology Laboratory (INL)
Avenida Mestre José Veiga
Braga 4715-310, Portugal

Prof. J. Fernández-Rossier
Departamento de Física Aplicada
Universidad de Alicante
San Vicente del Raspeig, Alicante 03690, Spain

states if time reversal symmetry is preserved. In-gap YSR states have now been observed in a variety of systems that integrate superconductors with magnetic moments in the form of molecules,[7] self-assembled,[8] and artificial atomic chains,[9] magnetic islands,[10,11] and also in proximity-induced superconducting molecular break junctions.[12] Current interest in YSR states is driven by their potential to induce a topological phase transition in the superconductor.[8,13] leading to the appearance of Majorana modes with potential application in topological quantum computing.[14–17]

A priori, chemically pure graphene is far from being an optimal system to look for YSR states, as it lacks both superconductivity and magnetism. However, superconductivity can be induced in graphene via proximity effect[18–20] and magnetism is expected to occur in graphene grain boundaries (GBs).[21–25] YSR states were predicted[26] to occur in graphene endowed with a superconducting proximity gap when a local moment is induced by chemisorption of individual hydrogen atoms, which are known to lead to the emergence of magnetic moments.[27]

Given the ubiquity of graphene GBs, it is of the utmost importance to obtain unequivocal experimental evidence of the presence of local moments. Here, we assess this matter by inducing superconductivity in the GB via proximity effect and exploring the emergence of YSR states by means of STS spectroscopy. By so doing , we demonstrate that magnetism can coexist with proximity induced superconductivity, realizing exotic electronic phases in carbon-only structures, which complements the ongoing efforts along this line using twisted bilayer graphene.[28,29]

2. Results

We grow several layers of graphene on a SiC(000-1) substrate. In this system, the rotational disorder of the graphene layers electronically decouples π bands, leading to a stacking of essentially isolated graphene sheets.[30–32] The graphene layer on the surface is neutral, with 100–500 nm wide single-crystal domains of different crystallographic orientations,[33] see Experimental Section and Figure S1 (Supporting Information). On this graphene surface, we deposit 5–15 monolayers (ML) of Pb at a rate of 3–10 ML min^{-1} while maintaining the sample at room temperature.[34,35] As a result, several triangular Pb islands with heights between 2 and 10 nm and sides between 20 and 300 nm are formed, see **Figure 1**a.

We carry out STS of the electronic properties of graphene in the vicinity of the Pb islands to measure the strength of the superconducting proximity coupling. We acquire conductance

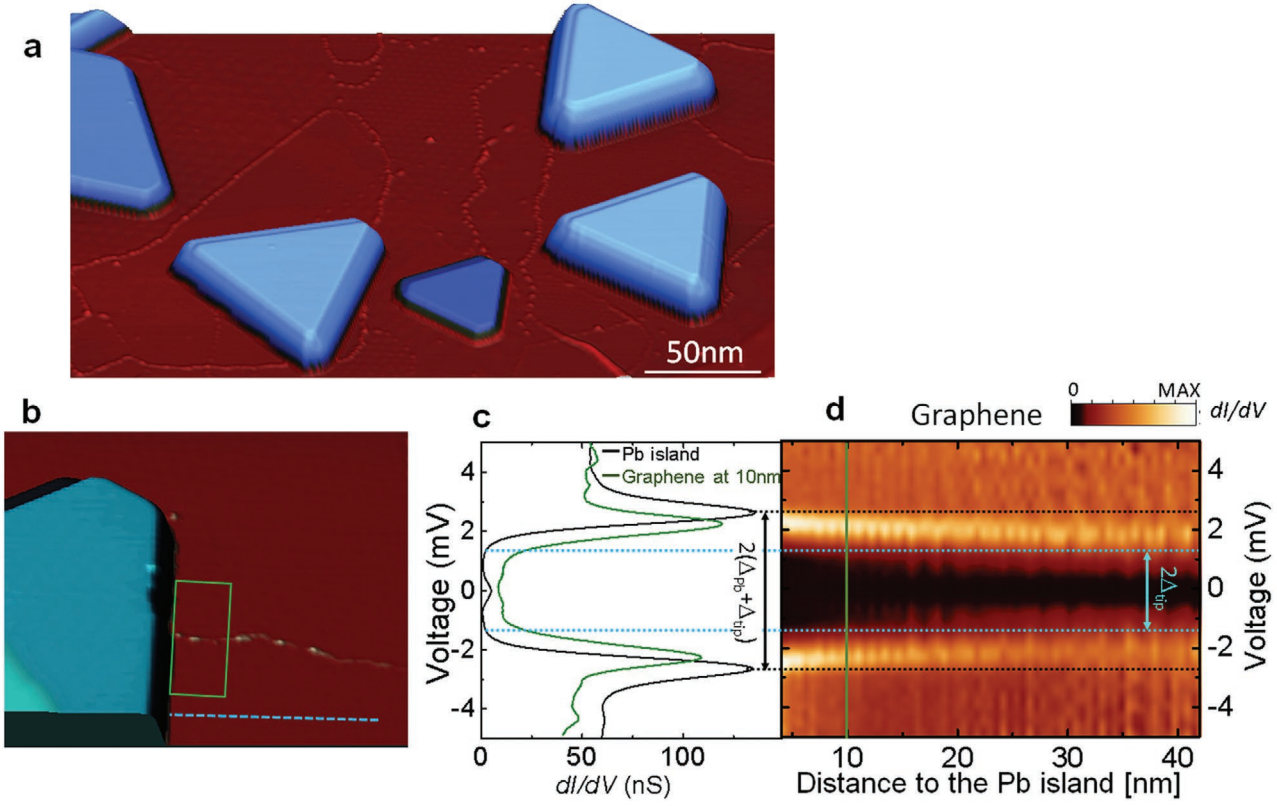

Figure 1. Graphene superconductivity induced by Pb islands. a) Large-scale STM image showing the general morphology of the sample after Pb deposition. Triangular-shaped Pb islands are formed on top of the graphene surface grown on SiC(000-1). In the image, several GBs are also be observed. b) STM image showing a Pb island on a graphene region with a GB. c) dI/dV spectra measured on the Pb island (black line) and on the pristine graphene region at 10 nm from it (green line), V_{bias} = 10 mV; I_{set}= 0.5 nA. d) Conductance map [dI/dV(x,E)] along the dashed line in (b) showing how SC is induced in pristine graphene close to the Pb island and far away from the GB (V_{bias} = 10 mV; I_{set} = 0.5 nA). Horizontal dotted lines indicate the Pb island SC gap, Δ_{Pb} (black line), and the SC tip gap Δ_{tip}, (blue line). The vertical green line corresponds to the graphene spectrum of (c). STS data are measured with a SC tip at T_s = 4 K; T_{tip} = 3 K. All the STM data were measured using the WSxM software.[36]

dI/dV curves, which probe the energy-resolved local density of states (LDOS(E)) under the tip position, as a function of the distance to the Pb islands. Our base experimental temperatures are: T_{sample} = 4 K, way below the Pb superconducting T_c = 7.2 K, and T_{tip} = 3 K. To increase the energy resolution beyond the thermal limit, we acquire STS spectra using SC Pb tips,[13,37] see Supporting Information and Figure S2 (Supporting Information). The conductance map, dI/dV(x,E), plotted with respect to distance to the Pb island and energy in Figure 1d, shows that a slowly decaying SC gap is induced in the pristine area of graphene, extending several tens of nanometers away from the Pb island edge, see also dI/dV spectra in Figure 1c and Figure S3 (Supporting Information). Our temperature dependent data shows that, since graphene is a 2D metal with a rather low charge carrier density, there is an almost negligible inverse proximity and the superconductivity in the Pb islands, remaining almost intact and very similar to bulk, see Supporting Information and Figure S4a,b (Supporting Information). As expected, the existence of SC in graphene is linked to the SC in the Pb island from where it inherits SC properties, see Figure S4c in the Supporting Information.

We now turn our attention to the STS on the GB of our superconducting graphene. Graphene GBs are naturally formed at the frontiers where the different graphene domains meet. These boundary regions present a rich structure characterized by the presence of many under-coordinated carbon atoms,[22,24,25,33] usually seen as bright features in STM images (Figures 1a,b,2a; Figures S1 and S7, Supporting Information). An atomically resolved STM image of the graphene GB highlighted by a green rectangle in Figure 1b, is shown in **Figure 2**a. The GB horizontally crosses the middle of the image, separating two graphene grains with 25° atomic lattice misalignment [see Figure 2b and Figure S7 (Supporting Information)]. A 3.2 nm height Pb island, perpendicularly crossing the GB on the left side, induces SC in the graphene region, see Figure 1b–d.

Our STS dI/dV spectra (Figure 2c), acquired moving the STM tip in the direction perpendicular to the graphene GB at a constant distance of 10 nm from the Pb island—along the green dotted line in Figure 2a, show the unambiguous presence of in-gap YSR states in the graphene GB (see also point spectra in Figure 2d). The evolution of the dI/dV spectra as the STM moves perpendicular to the graphene GB, show how the amplitude of the YSR features is maximal at the graphene GB and decays as the tip enters into the pristine graphene areas. The extension of the YSR feature in that direction is at least 20 nm (Figure 2e), with a more rapid decay in the lower graphene domain. The asymmetry on the decay of the YSR modes stems from the sublattice structure of the magnetic response of graphene. In particular, in the zigzag region, upper domain, RKKY favors a relatively long decay length of the magnetic order, whereas, in the armchair part, lower domain, the RKKY interaction quickly quenches the magnetic order. These different penetration lengths of the magnetic order ultimately impact the decay of the Yu–Shiba–Rusinov peaks.

The spatial extension of these YSR states is much larger than the one reported by Menard et al. in the case of magnetic dopants in 2D $NbSe_2$[42] that in turn is much larger than the ones reported in 3D superconductors. Moreover, the YSR state features a $\sqrt{3} \times \sqrt{3}$ modulation along the direction rotated 30° with respect to the atomic lattice, see Figure 2e. Such modulation, associated to the wave vector which spans the two valleys in the Brillouin zone, is also observed in the resonance magnetic states generated close to the Fermi level (E_F) by atomically sharp impurities in graphene,[27] and reflects in both cases the sublattice dependent response of graphene to local perturbations.

Further experimental evidence of the magnetic origin of the in-gap features observed at the GB can be obtained from STS carried out by increasing the temperature above the superconducting T_c, so that superconducting order is suppressed. This brings graphene to its normal phase. In this situation, both the gap and the sharp in-gap state completely disappear (see Figure 2f and Figure S4d (Supporting Information)). In addition, we have measured temperature dependent spectra on a larger voltage scale (see Figure 2g). Our dI/dV spectra on the graphene GB show the presence of two additional broad peaks, one below and one above E_F, at energies well beyond the SC gap. We ascribe those peaks to the addition/removal quasiparticle peaks in localized states, whose splitting comes mostly from the Coulomb repulsion.[27,38,39] Consistent with this assumption, our data show that, contrary to the in-gap states, such peaks are essentially independent to temperature changes throughout graphene SC transition, see Figure 2g. Information about the precise magnetic structure of the YSR states could be obtained by spin-polarized measurements of the in-gap states.[8]

In order to determine the actual density of states (DOS), we have to carry out a numerical deconvolution of the dI/dV curves to remove the features that arise from the tip superconducting gap, see methods section for details. The deconvoluted curves so obtained provide a faithful representation of the surface DOS having performed the measurements with a superconducting tip, and permit to address the energy of the YSR states inside the gap.

The hallmark of YSR states are pairs of peaks with energy $E_B < \Delta$ symmetrically located around $E_F = 0$, but with asymmetric height, on account of their different electron–hole weight. In the case of the GB shown in Figure 2, the YSR state correspond to a state with $E_B \approx 0$, as shown in the deconvoluted spectra of the middle panel of **Figure 3**b, see also Figure S8 (Supporting Information). Different spectra, with $E_B \neq 0$, are obtained, depending on the GB-Pb island configuration and the location of the boundary probed, see Figure 3 and Figure S9 (Supporting Information). The variation in energy of the bound state suggests that the strength of the interaction induced exchange coupling depends on the actual details of the interface.

In general, the number of YSR states, and their binding energies, depend both on the internal structure of the magnetic impurity and on the strength of the exchange coupling J between the local spin and the surface electrons. Thereby, in other systems, for the same magnetic species placed in different adsorption sites of the surface of a conventional SC, different YSR spectra were also reported.[7,13] Depending on the strength of J, the parity of the ground state of the system can be different. In the weak exchange coupling limit, the BCS condensate remains in the spin $S = 0$ limit, and the multiplicity of the state is given by the one of the local moment. However, at some critical value of J a Cooper pair is broken, so that the BCS condensate has $S = 1/2$. The critical point is marked by a YSR with $E_B = 0$.[40,41]

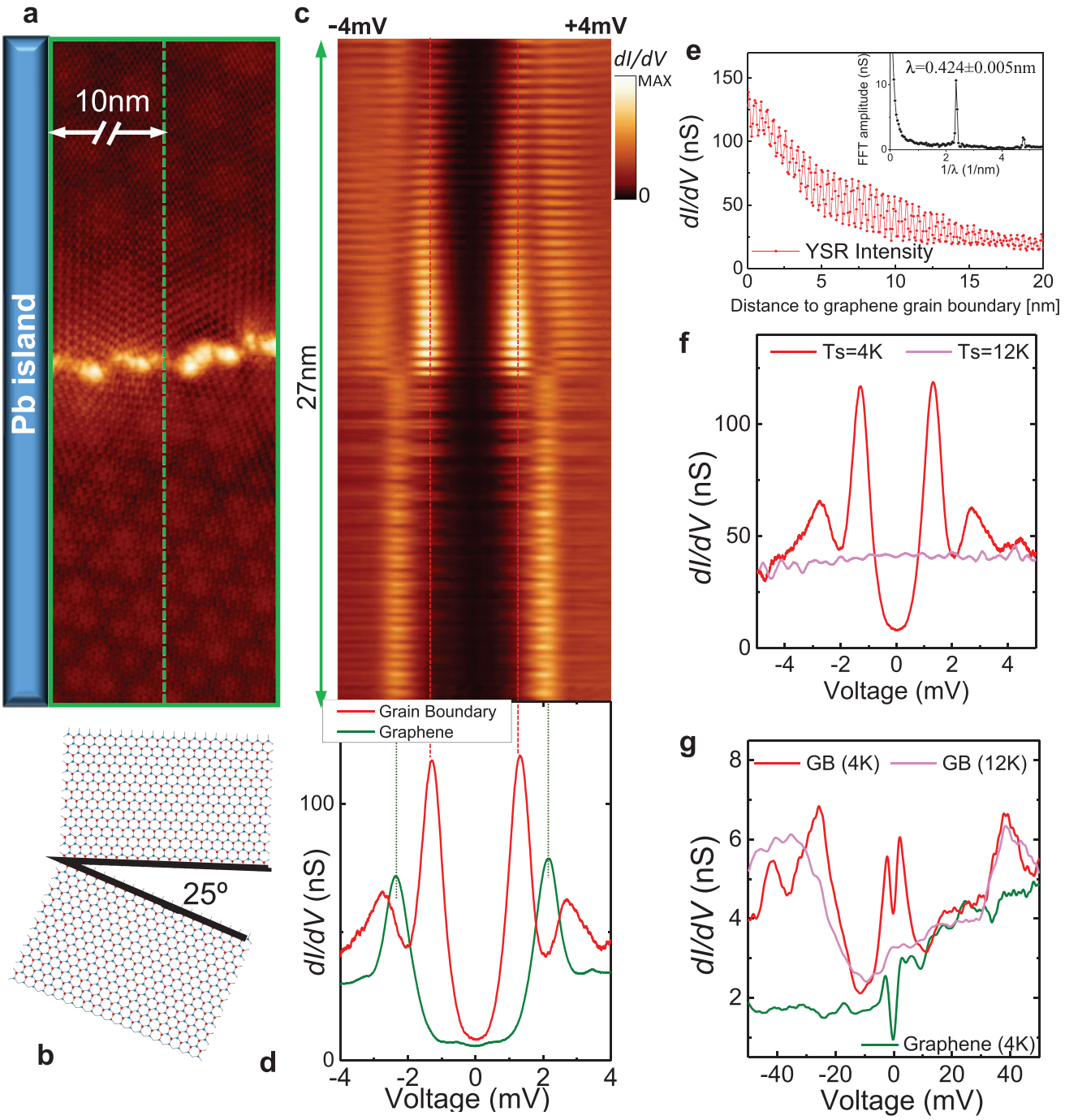

Figure 2. GB magnetism induces Yu–Shiba–Rusinov states in superconducting graphene. a) Atomically resolved topography showing a zoom in of the GB outlined by the green rectangle in Figure 1b. Superconductivity is induced in the region by a Pb island placed at the left of the image. Size: 7.5×27 nm^2. b) Schematic of the orientation of the graphene domains in (a), showing the 25° rotation between them. c) Conductance map [$dI/dV(x,E)$], measured with an SC tip, along the line crossing the GB, highlighted in green in (a) (V_{bias} = 12 mV; I_{set} = 0.5 nA). The line is parallel to the $\sqrt{3}\times\sqrt{3}$ direction of the upper graphene grain and to the Pb island (at a constant distance of 10 nm). The vertical dotted lines outline the YSR in-gap states. d) Single dI/dV spectra on top of the GB (red line) and on pristine graphene (green line), both measured at a 10 nm distance from the Pb island (V_{bias} = 12 mV; I_{set} = 0.5 nA). e) Spatial extension of the in-gap YSR state and $\sqrt{3}\times\sqrt{3}$ modulation. The graph corresponds to a measurement of the dI/dV YSR peak intensity as a function of the distance to the GB, on the upper graphene grain, along the same direction outlined by the green line in (a). The inset shows the 1D-FT of the YSR intensity profile. A periodicity of $\lambda = 0.424 \pm 0.005$ nm is found, in agreement with the $\lambda = 0.426$ nm of the $\sqrt{3}\times\sqrt{3}$ periodicity. f) dI/dV spectra measured on the same spot of the GB for temperatures both below (red) and above (pink) the superconducting transition (V_{bias} = 12 mV; I_{set} = 0.5 nA). YSR in-gap state completely vanishes for $T > T_c$ (pink curve). g) dI/dV spectra on a higher energy scale (V_{bias} = 50 mV; I_{set} = 0.25 nA). On the GB (red and pink curves), besides the YSR state, two broader peaks at higher energies are also observed. Those peaks, ascribed to GB magnetism, are essentially unaltered through the SC phase transition.

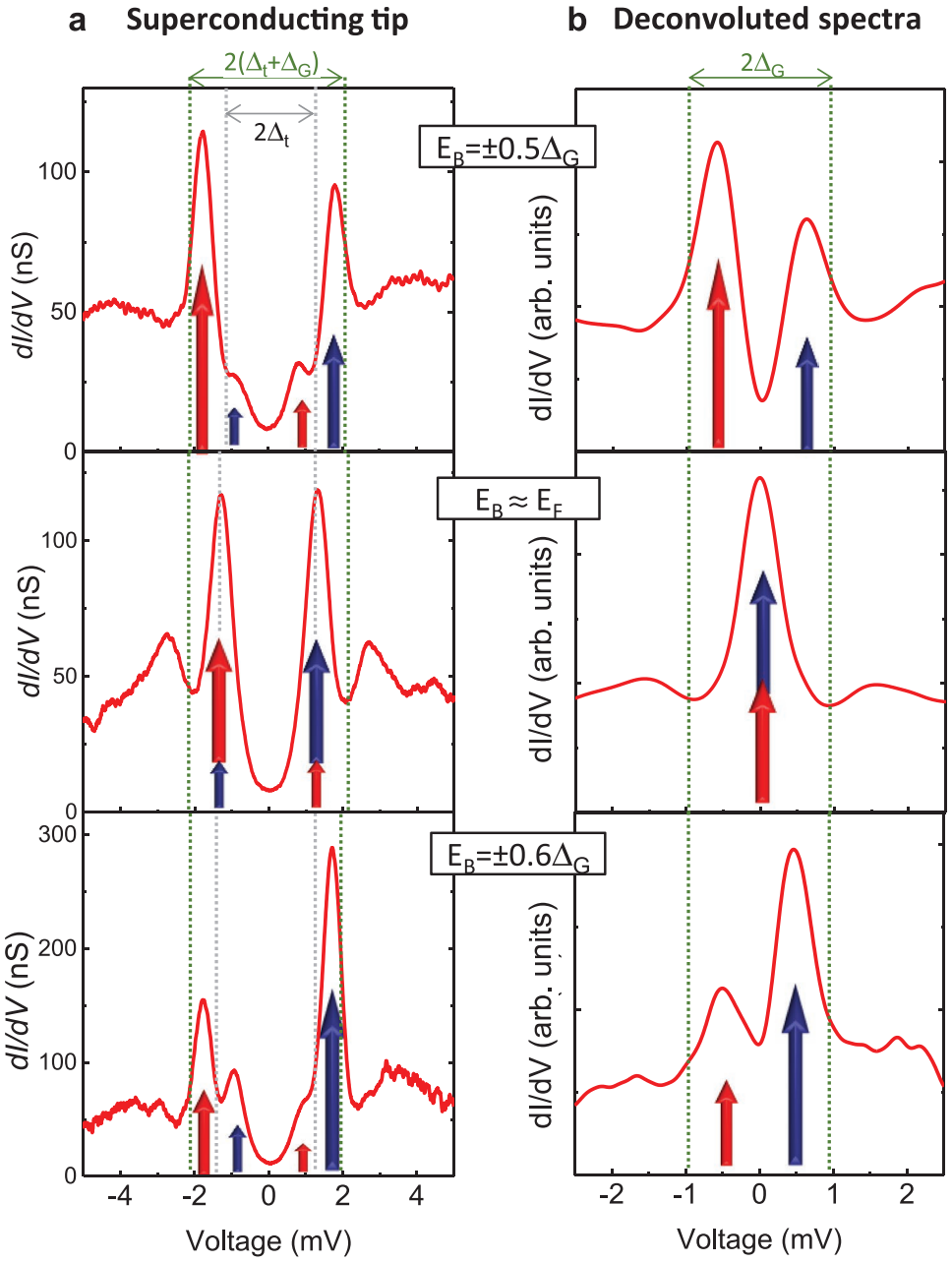

Figure 3. Yu–Shiba–Rusinov states in graphene for different GB configurations. a) d*I*/d*V* spectra measured, with a SC tip, on 3 characteristic GB configurations (stabilization values for the up, middle, and bottom spectra are V_{bias} = 10 mV; I_{set} = 0.5 nA; V_{bias} = 12 mV; I_{set} = 0.5 nA; V_{bias} = 6 mV; I_{set} = 0.5 nA respectively). Outer vertical dotted lines outline the energy position of $\Delta_{tip} + \Delta_G$. Inner vertical dotted lines outline the energy position of Δ_{tip}. In the spectra, 4 in-gap peaks, outlined by red and blue arrows, are clearly resolved. The 2 outer ones, with larger amplitudes, correspond to the electron and hole-like components of the YSR excitation. The 2 inner ones, at $E < \Delta_{tip}$ and with much smaller amplitudes, are due to the thermally activated tunneling occurring at finite temperatures, see Supporting Information and Figures S5, S6, and S9 (Supporting Information). B) Corresponding GB d*I*/d*V* spectra, obtained by numerical deconvolution of STS data in (a). Vertical dotted lines outline the energy position of Δ_G.

3. Discussion

The nature of the YSR states reported here is peculiar on several counts. First, the YSR states are observed in a chemically homogeneous region, made of carbon only and free of other chemical species. Second, they are observed in graphene, that has to borrow superconductivity from Pb islands located several nanometers away. Third, YSR states present an extremely large spatial extension, on account of the 2D nature of graphene.[42]

In order to provide a theoretical basis to this completely novel scenario, we model the GB using a Hubbard model plus a pairing BCS term $\mathcal{H} = \Sigma_{i,i',\sigma} t_{ii'} c^{\dagger}_{i\sigma} c_{i'\sigma} + U\Sigma_i n_{i\uparrow} n_{i\downarrow} + \Delta\Sigma_i c^{\dagger}_{i\uparrow} n c^{\dagger}_{i\downarrow} + h.c.$ We consider a GB between a zigzag and an armchair oriented

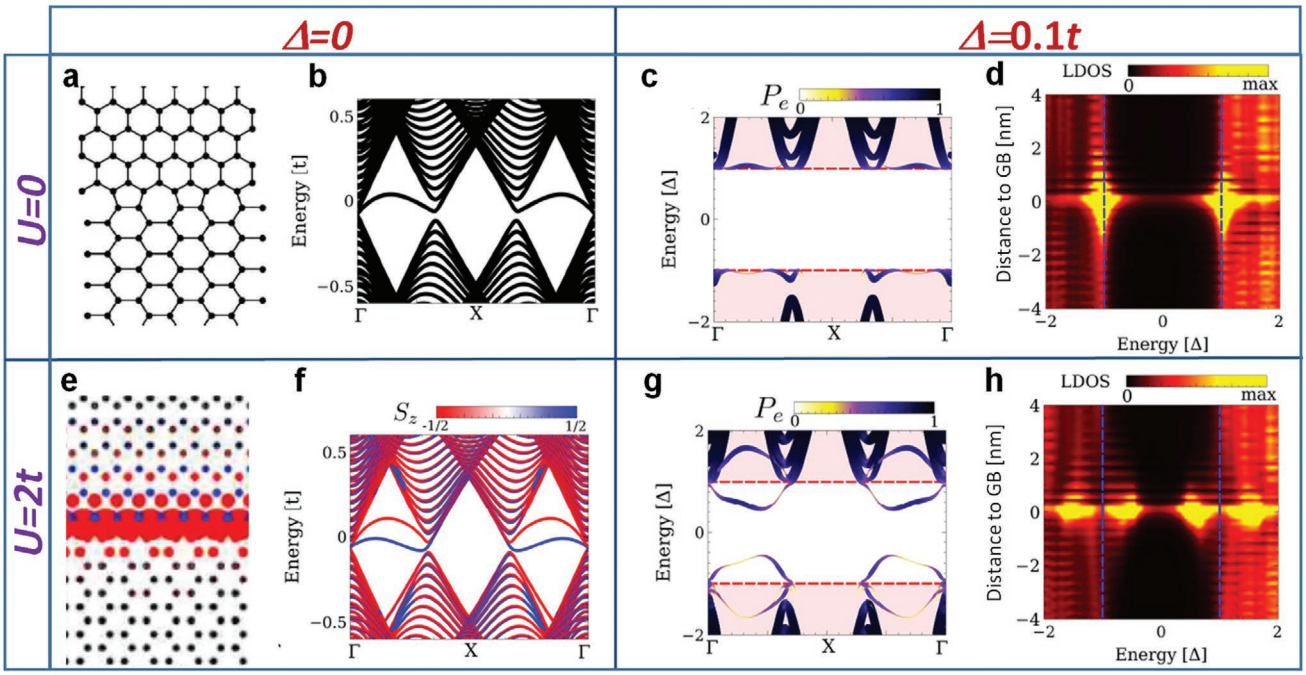

Figure 4. Interface between an armchair and zigzag oriented regions. a) Atomic structure of the GB. b) Such GB hosts a nearly flat band as shown. c,d) When superconducting proximity effect is introduced, in the absence of magnetism, no in-gap state is observed as shown in the band structure (c) and in the spatially resolved DOS (d). e,f) Upon inclusion of interactions, the GB becomes magnetic, with the appearance of local magnetic moments (e) and the spin-splitting of the band structure (f). The area of each circle in (e) is proportional to the amplitude of the local magnetic moment at each atom. g,h) When superconducting proximity effect is introduced on top of the magnetic state, in-gap YSR bands appear. P_e denotes the projection of the state in the electron-sector of the Bogoliubov–de Gennes Hamiltonian, which are the states accessible in STM spectroscopy.

ribbons, **Figure 4**a. The mismatch angle is 30°, close to the one observed experimentally. Taking $U = \Delta = 0$, the single particle bands feature a narrow band associated to states located at the GB, see Figure 4b. When a finite value of $U = 2t$ is considered, in the mean field approximation, still with $\Delta = 0$, we find the emergence of a spin-splitting in the band structure (Figure 4f) associated to magnetism in the GB, as shown in Figure 4e. Let us now move to the case with a proximity induced superconducting pairing stemming from the Pb islands, focusing first on the non-magnetic situation. In this case, in which we ignore electronic interactions, the interface remains non-magnetic, giving rise to a superconducting gap everywhere as shown in Figure 4c. In stark contrast, when we consider the magnetic case with superconducting proximity effect (Figure 4g), we observe the emergence of the in-gap Yu–Shiba–Rusinov states inside the superconducting gap.

It is also informative to look at the density of states as a function to the distance to the GB, as shown in Figure 4d,h. In the presence of superconductivity, in-gap resonances at the GB appears when the interaction-induced magnetism is included (Figure 4h), whereas no in-gap resonance appears in the absence of magnetism (Figure 4d). The apparent finite weight inside the gap that can be appreciated in Figure 4d, is just an effect of the finite energy smearing used in the calculation to mimic the thermal smearing in the experiment. The decay length of the Shiba state is significantly shorter in theory than in experiments. This is due to the choice of the magnitude of the superconducting gap, which governs the extension of the YSR state as shown in Figure S10 in the Supporting Information.

There are several features to highlight. First, the YSR peaks show a weak electron–hole asymmetry in line with experimental observations, which can be related to the breakdown of the bipartite character of the GB, leading to single-particle states without electron–hole symmetry. Second, the location in energy of the in-gap states depends on details of the interface, such as the strength of the interaction-induced exchange coupling, or the specific geometry of the GB, see Figures S10–S12 (Supporting Information) for details. We note that our calculations do not incorporate the effect of chemical reconstructions, but rather focus on the fundamental mechanism in which an interface-defect gives rise to YSR states. Finally, the emergence of flat bands and magnetism orientation interfaces are generic features of GBs, beyond the specific case considered here. This stems from the Berry phase mismatch between the orientations, which enforces the emergence of flat band states for a generic chiral interface.[43]

4. Conclusion

We have used Pb islands to induce superconductivity in graphene, exploiting GB as a source of local magnetic moments to realize, for the first time, YSR states in graphene. Importantly, our experiments provide an unequivocal proof of carbon magnetism at graphene GBs, as the emergence of in-gap state in the presence of superconductivity demonstrate the interaction with local magnetic moments. Finally, our results provide a starting point towards the exploration of exotic electronic

phases involving both magnetism and superconductivity in graphene that, together with further proximity to strong spin–orbit coupling materials, may lead to the emergence of topological superconductivity at graphene GBs.

5. Experimental Section

Sample Preparation and Experimental Details: All the preparation procedures and measurements were performed under UHV conditions. During the whole process—imaging pristine graphene sample = > depositing Pb on it = > and imaging it back—the sample was maintained in the same UHV system.

The multilayer graphene substrate was grown on a 6H-SiC(000-1) sample (C face) following the method described.[44] This process takes place in a RF furnace. In brief, it consists in heating (at 1600 °C) the SiC substrate held in a graphite crucible under an Ar atmosphere (1 bar Ar) for 30 min. Before this graphitization step, the substrate is etched in an Ar/H2 mixture.[45] After the growth, the sample is transferred into a separate ultrahigh vacuum (UHV) setup and outgazed.

The graphene layer on the surface has 100–500 nm wide single-crystal domains of different crystallographic orientations.[33] On the surface, graphene GBs are naturally formed at the frontier between these pristine graphene domains with different crystallographic orientations. These boundary regions are usually seen as bright features in STM images (see GBs outlined by arrows in Figure S1 in the Supporting Information).

In this system, the rotational disorder of the graphene layers electronically decouples π bands leading to a stacking of essentially isolated graphene sheets.[30–32] The pristine graphene surface layer is essentially neutral, presenting a very low electron doping[34] ($<3 \times 10^{11}$ cm^{-2}) as deduced from the quasiparticle interference (QPI) pattern measurements[46,47] and from the position of the Van Hove singularities associated with the moiré pattern.[32,48] On this graphene surface, 5–15 monolayers (ML) of Pb at a rate of 3–10 ML min^{-1} while maintaining the sample at RT.[34] The thickness of the islands in monolayer (ML) units is obtained by dividing their apparent height as measured by STM by the Pb (111) interlayer distance (0.286 nm). As a result, several triangular Pb islands with heights between 2 and 10 nm and sides between 20 and 300 nm are formed, see Figure S1 in the Supporting Information.

Method for the Numerical Deconvolution of the Experimental dI/dV Data: In order to increase the energy resolution beyond the thermal limit,[13,37] STS data using SC Pb tips are acquired. Therefore, to determine the actual density of states (DOS), a numerical deconvolution of the dI/dV curves to remove the features that arise from the tip superconducting gap. The deconvolution is performed by defining a functional $S = \int_{-\infty}^{\infty} dw[g_{th}(w) - g_{exp}(w)]^2$, where $g_{exp}(w)$ is the experimentally measured dI/dV and $g_{th}(w)$ is the theoretically expected dI/dV of the form $g_{th}(w) = \frac{\partial}{\partial w} \int dw' D_{tip}(w+w') D_{surface}(w')[1 - n_{tip}(w+w')] n_{surface}(w)$, where D_{tip} is the density of states of the tip (which is known) and $D_{surface}$ the density of states of the surface. The density of states of the surface is computed by minimizing the functional S as $\frac{\delta S}{\delta D_{surface}} = 0$. The deconvoluted curves so obtained provide a faithful representation of the surface DOS having performed the measurements with a superconducting tip, and permit to address the energy of the YSR states inside the gap.

Supporting Information

Supporting Information is available from the Wiley Online Library or from the author.

Acknowledgements

The authors thank J-I. Pascual and E. Lee for fruitful discussions. This work was supported by AEI and FEDER under projects MAT2016-80907-P and MAT2016-77852-C2-2-R (AEI/FEDER, UE), by the Fundación Ramón Areces, and by the Comunidad de Madrid NMAT2D-CM program under grant S2018/NMT-4511. J.F.R. acknowledges financial support European Regional Development Fund Project No. NORTE-01-50145-FEDER-000019, and the UTAPEXPL/NTec/0046/2017 projects, as well as Generalitat Valenciana funding Prometeo2017/139 and MINECO Spain (Grant No. MAT2016-78625-C2). J.L.L is grateful for financial support from the Academy of Finland Projects Nos. 331342 and 336243.

Conflict of Interest

The authors declare no conflict of interest.

Data Availability Statement

The data that support the findings of this study are available from the corresponding author upon reasonable request.

Keywords

graphene, grain boundaries, magnetism, superconductivity, topology, Yu–Shiba–Rusinov states

Received: December 1, 2020
Revised: February 26, 2021
Published online: April 23, 2021

[1] J. Bardeen, L. N. Cooper, J. R. Schrieffer, *Phys. Rev.* **1957**, *108*, 1175.
[2] L. Yu, *Acta Phys. Sin.* **1965**, *21*, 75.
[3] H. Shiba, *Prog. Theor. Phys.* **1968**, *40*, 435.
[4] A. I. Rusinov, *Sov. J. Exp. Theor. Phys* **1969**, *29*, 1101.
[5] A. Yazdani, B. A. Jones, C. P. Lutz, M. F. Crommie, D. M. Eigler, *Science* **1997**, *275*, 1767.
[6] P. W. Anderson, *J. Phys. Chem. Solids* **1959**, *11*, 26.
[7] K. J. Franke, G. Schulze, J. I. Pascual, *Science* **2011**, *332*, 940.
[8] S. Nadj-Perge, I. K. Drozdov, J. Li, H. Chen, S. Jeon, J. Seo, A. H. MacDonald, B. A. Bernevig, A. Yazdani, *Science* **2014**, *346*, 602.
[9] H. Kim, A. Palacio-Morales, T. Posske, L. Rózsa, K. n. Palotás, L. s. Szunyogh, M. Thorwart, R. Wiesendanger, *Sci. Adv.* **2018**, *4*, eaar5251.
[10] A. Palacio-Morales, E. Mascot, S. Cocklin, H. Kim, S. Rachel, D. K. Morr, R. Wiesendanger, *Sci. Adv.* **2019**, *5*, eaav6600.
[11] S. Kezilebieke, M. N. Huda, V. Vano, M. Aapro, S. C. Ganguli, O. J. Silveira, S. Glodzik, A. S. Foster, T. Ojanen, P. Liljeroth, *Nature* **2020**, *588*, 424.
[12] J. O. Island, R. Gaudenzi, J. de Bruijckere, E. Burzua, C. Franco, M. Mas-Torrent, C. Rovira, J. Veciana, T. M. Klapwijk, R. n. Aguado, H. S. â. J. van der Zant, *Phys. Rev. Lett.* **2017**, *118*, 117001.
[13] B. W. Heinrich, J. I. Pascual, K. J. Franke, *Prog. Surf. Sci.* **2018**, *93*, 1.
[14] S. D. Sarma, M. Freedman, C. Nayak, *npj Quantum Inf.* **2015**, *1*, 15001.
[15] D. Chatzopoulos, D. Cho, K. M. Bastiaans, G. O. Steffensen, D. Bouwmeester, A. Akbari, G. Gu, J. Paaske, B. M. Andersen, M. P. Allan, *Nat. Commun.* **2021**, *12*, 298.
[16] P. Fan, F. Yang, G. Qian, H. Chen, Y.-Y. Zhang, G. Li, Z. Huang, Y. Xing, L. Kong, W. Liu, K. Jiang, C. Shen, S. Du, J. Schneeloch,

R. Zhong, G. Gu, Z. Wang, H. Ding, H.-J. Gao, *Nat. Commun.* **2021**, *12*, 1348.
[17] D. Wang, J. Wiebe, R. Zhong, G. Gu, R. Wiesendanger, *Phys. Rev. Lett.* **2021**, *126*, 076802.
[18] H. B. Heersche, P. Jarillo-Herrero, J. B. Oostinga, L. M. K. Vandersypen, A. F. Morpurgo, *Nature* **2007**, *446*, 56.
[19] F. D. Natterer, J. Ha, H. Baek, D. M. Zhang, W. G. Cullen, N. B. Zhitenev, Y. Kuk, J. A. Stroscio, *Phys. Rev. B* **2016**, *93*, 4.
[20] G. H. Lee, H. J. Lee, *Rep. Prog. Phys.* **2018**, *81*, 056502.
[21] J. Cervenka, M. I. Katsnelson, C. F. J. Flipse, *Nat. Phys.* **2009**, *5*, 840.
[22] S. Dutta, K. Wakabayashi, *Sci. Rep.* **2015**, *5*, 11744.
[23] D. Martínez-Martín, M. Jaafar, R. Pérez, J. Gómez-Herrero, A. Asenjo, *Phys. Rev. Lett.* **2010**, *105*, 257203.
[24] A. Mesaros, D. Sadri, J. Zaanen, *Phys. Rev. B* **2010**, *82*, 205119.
[25] M. A. Akhukov, A. Fasolino, Y. N. Gornostyrev, M. I. Katsnelson, *Phys. Rev. B* **2012**, *85*, 115407.
[26] J. L. Lado, J. Fernandez-Rossier, *2D Mater.* **2016**, *3*, 025001.
[27] H. González-Herrero, J. M. Gómez-Rodríguez, P. Mallet, M. Moaied, J. J. Palacios, C. Salgado, M. M. Ugeda, J.-Y. Veuillen, F. Yndurain, I. Brihuega, *Science* **2016**, *352*, 437.
[28] Y. Cao, V. Fatemi, S. Fang, K. Watanabe, T. Taniguchi, E. Kaxiras, P. Jarillo-Herrero, *Nature* **2018**, *556*, 43.
[29] A. L. Sharpe, E. J. Fox, A. W. Barnard, J. Finney, K. Watanabe, T. Taniguchi, M. A. Kastner, D. Goldhaber-Gordon, *Science* **2019**, *365*, 605.
[30] M. Sprinkle, D. Siegel, Y. Hu, J. Hicks, A. Tejeda, A. Taleb-Ibrahimi, P. L.e Fevre, F. Bertran, S. Vizzini, H. Enriquez, S. Chiang, P. Soukiassian, C. Berger, W. A. de Heer, A. Lanzara, E. H. Conrad, *Phys. Rev. Lett.* **2009**, *103*, 226803.
[31] G. H. Li, A. Luican, J. dos Santos, A. H. C. Neto, A. Reina, J. Kong, E. Y. Andrei, *Nat. Phys.* **2010**, *6*, 44.
[32] I. Brihuega, P. Mallet, H. González-Herrero, G. T. de Laissardière, M. M. Ugeda, L. Magaud, J. M. Gómez-Rodríguez, F. Yndurain, J. Y. Veuillen, *Phys. Rev. Lett.* **2012**, *109*, 196802.
[33] F. Varchon, P. Mallet, L. Magaud, J. Y. Veuillen, *Phys. Rev. B* **2008**, *77*, 165415.
[34] V. Cherkez, P. Mallet, T. L.e Quang, L. Magaud, J. Y. Veuillen, *Phys. Rev. B* **2018**, *98*, 195441.
[35] F. Paschke, T. Birk, S. Forti, U. Starke, M. Fonin, *Adv. Quantum Technol.* **2020**, *3*, 2000082.
[36] I. Horcas, R. Fernández, J. M. Gómez-Rodríguez, J. Colchero, J. Gómez-Herrero, A. M. Baró, *Rev. Sci. Instrum.* **2007**, *78*, 013705.
[37] J. G. Rodrigo, H. Suderow, S. Vieira, *Eur. Phys. J. B* **2004**, *40*, 483.
[38] A. Luican-Mayer, J. E. Barrios-Vargas, J. T. Falkenberg, G. Autes, A. W. Cummings, D. Soriano, G. Li, M. Brandbyge, O. V. Yazyev, S. Roche, E. Y. Andrei, *2D Mater.* **2016**, *3*, 031005.
[39] R. Ortiz, J. Fernández-Rossier, *arXiv:2002.07721,* **2020**.
[40] A. V. Balatsky, I. Vekhter, J.-X. Zhu, *Rev. Mod. Phys.* **2006**, *78*, 373
[41] L. t. Farinacci, G. Ahmadi, G. l. Reecht, M. Ruby, N. Bogdanoff, O. Peters, B. W. Heinrich, F. von Oppen, K. J. Franke, *Phys. Rev. Lett.* **2018**, *121*, 196803.
[42] G. C. Ménard, S. Guissart, C. Brun, S. Pons, V. S. Stolyarov, F. Debontridder, M. V. Leclerc, E. Janod, L. Cario, D. Roditchev, P. Simon, T. Cren, *Nat. Phys.* **2015**, *11*, 1013.
[43] P. Delplace, D. Ullmo, G. Montambaux, *Phys. Rev. B* **2011**, *84*, 195452.
[44] T. L. Quang, *Ph.D. Thesis*, Université Grenoble Alpes **2016**.
[45] K. V. Emtsev, A. Bostwick, K. Horn, J. Jobst, G. L. Kellogg, L. Ley, J. L. McChesney, T. Ohta, S. A. Reshanov, J. Rohrl, E. Rotenberg, A. K. Schmid, D. Waldmann, H. B. Weber, T. Seyller, *Nat. Mater.* **2009**, *8*, 203.
[46] I. Brihuega, P. Mallet, C. Bena, S. Bose, C. Michaelis, L. Vitali, F. Varchon, L. Magaud, K. Kern, J. Y. Veuillen, *Phys. Rev. Lett.* **2008**, *101*, 206802.
[47] P. Mallet, I. Brihuega, S. Bose, M. M. Ugeda, J. M. Gómez-Rodríguez, K. Kern, J. Y. Veuillen, *Phys. Rev. B* **2012**, *86*, 045444.
[48] V. Cherkez, G. T. Laissardière, P. Mallet, J.-Y. Veuillen, *Phys. Rev. B* **2015**, *91*, 155428.